Designing Narcissistic Self-Sorting Terpyridine Moieties with High Coordination Selectivity for Complex Metallo-Supramolecules

Jianjun Ma
State Key Laboratory of Supramolecular Structure and Materials, College of Chemistry, Jilin University
https://orcid.org/0000-0002-2563-6369

Tong Lu
State Key Laboratory of Supramolecular Structure and Materials, College of Chemistry, Jilin University

Xiaozheng Duan
Changchun Institute of Applied Chemistry

Yaping Xu
State Key Laboratory of Supramolecular Structure and Materials, College of Chemistry, Jilin University
https://orcid.org/0000-0002-7492-755X

Zhikai Li
College of Chemistry and Environmental Engineering, Shenzhen University https://orcid.org/0000-0002-9781-2747

Kehuan Li
State Key Laboratory of Supramolecular Structure and Materials, College of Chemistry, Jilin University
https://orcid.org/0000-0001-6403-2616

Junjuan Shi
State Key Laboratory of Supramolecular Structure and Materials, College of Chemistry, Jilin University
https://orcid.org/0000-0003-2564-5975

Qixia Bai
Institute of Environmental Research at Greater Bay Area, Guangzhou University https://orcid.org/0000-0003-3995-5616

zhe zhang
Guangzhou University

Xin-Qi Hao
Zhengzhou University https://orcid.org/0000-0003-1942-8309

Zhi Chen
Shenzhen University

Pingshan Wang
Guangzhou University https://orcid.org/0000-0002-1988-7604

Ming Wang (mingwang358@jlu.edu.cn)

Jilin University https://orcid.org/0000-0002-5332-0804

Article

Keywords: Supramolecular self-assembly, self-sorting, terpyridine, coordination selectivity

Posted Date: July 16th, 2021

DOI: https://doi.org/10.21203/rs.3.rs-228339/v1

Version of Record: A version of this preprint was published at Communications Chemistry on September 24th, 2021. See the published version at https://doi.org/10.1038/s42004-021-00577-0.

Designing Narcissistic Self-Sorting Terpyridine Moieties with High Coordination Selectivity for Complex Metallo-Supramolecules

Jianjun Ma[1], Tong Lu[1], Xiaozheng Duan[2], Yaping Xu[1], Zhikai Li[3], Kehuan Li[1], Junjuan Shi[1], Qixia Bai[4], Zhe Zhang[4], Xin-Qi Hao[5], Zhi Chen[3], Pingshan Wang[4], and Ming Wang[1]*

[1] *State Key Laboratory of Supramolecular Structure and Materials, College of Chemistry, Jilin University, Changchun, Jilin 130012, China*

[2] *State Key Laboratory of Polymer Physics and Chemistry, Changchun Institute of Applied Chemistry, Chinese Academy of Sciences, Changchun, Jilin 130022, China*

[3] *College of Chemistry and Environmental Engineering, Shenzhen University, Shenzhen, Guangdong 518060, China*

[4] *Institute of Environmental Research at Greater Bay Area; Key Laboratory for Water Quality and Conservation of the Pearl River Delta, Ministry of Education; Guangzhou Key Laboratory for Clean Energy and Materials; Guangzhou University, Guangzhou, Guangdong 510006, China*

[5] *Green Catalysis Center, Henan Key Laboratory of Chemical Biology and Organic Chemistry, and College of Chemistry, Zhengzhou University, Zhengzhou, Henan 450001, China.*

E-mail: mingwang358@jlu.edu.cn (M. W.)

KEYWORDS: Supramolecular self-assembly, self-sorting, terpyridine, coordination selectivity

ABSTRACT： Coordination-driven self-assembly serves as a powerful approach for the construction of metallo-supramolecules, however, it still remains its infancy in design of coordination moieties with high selectivity and specificity. Herein, two unique ortho-modified terpyridine ligands (**MA** and **MB**) were designed and synthesized to form head-to-tail coordination complexes with Zn(II) respectively. Both of them showed excellent narcissistic self-sorting process due to the exquisite design. Further, two multitopic ligands (**LA** and **LB**) with narcissistic self-sorting moieties were obtained and used to construct more complex metallo-supramolecules hexagons. More interestingly, because of the non-coaxial structural restrictions in the rotation of terpyridine moieties, the obtained hexagonal macrocycles were able to hierarchically self-assemble into giant cyclic nanostructures via edge-to-edge stacking rather than face-to-face stacking. Our design of dissymmetrical coordination moieties could pave a new avenue for the development of congested coordination pairs with high selectivity and specificity.

Introduction

Coordination-driven self-assembly has been proven to be an effective approach for constructing supramolecular structures, due to its high predictability.[1-6] As such, a variety of discrete metallo-supramolecular architectures have been fabricated through different types of self-assembly strategies, including the coordinations of pyridyl,[7] bipyridyl,[8] terpyridyl[9] or heterotopic ligands[10-12] with naked metal ions or metal-organic components.[13-14] Given the increasing demands for diverse and predesigned molecular structures and functions, scientists are encouraged to further develop novel building blocks to achieve high coordination selectivity in precise and controllable supermolecular assembly.

2,2':6',2''-tpy and its derivatives have been widely employed in coordination-driven self-assembly on account of their variable coordination ability with transition metal ions, as well as the unique properties and wide applications in optical devices,[15] catalysis,[16] self-healing,[17] and drug delivery[18] after complexation. Among the design of tpy-based metallo-supramolecules, the most common strategy is connecting tpy units and directing units at the central pyridine for subsequent coordination, which usually caused the poor selectivity of coordination units.[4, 19-23] To further enhance geometrical diversity and complexity of assemblies, hierarchical stepwise assembly strategy has been developed to promote the controllability of self-assembly process by using metals that can form strong coordinative bonds with tpy, such as <tpy-Ru(II)-tpy> or <tpy-Fe(II)-tpy>.[9, 24-25] However, the tedious synthesis and column separation procedures limit its extensive application in supermolecular constructions.[25-27] Currently, it still remains a challenge to precisely construct complex supramolecular structures through the one-step method.

Nature has given us the enlightenment in the exploration of controllable self-assembly of supramolecules with the self-sorting process, such as the complementary pairing of DNA and the folding of polypeptides of proteins.[28] In recent years, much more attention has been paid to the design of different ligands for the diversity and controllability of supramolecular assembly through social self-discrimination or narcissistic self-recognition manner.[29-33] Particularly, social self-discrimination is relatively common

for tpy moieties, and multiple different building blocks can be engineered to form impressively complex structures.[34-35] For example, phenanthroline with modification at 2,9-positions and tpy with modification at 6,6"-position could show the complete social self-sorting behaviors when mixed with tpy (Scheme 1a).[36-37] In a recent review, Schmittel summarized a dynamic library formed by hetero-ligand motifs and introduced a lot of elegant structures constructed by the social self-sorting process.[38] In contrast, the narcissistic self-recognition manner for tpy moieties is rarely reported.[39-41] It has been more than twenty years since Lehn reported the first narcissistic self-sorting of a double helix, and there have also been many reports about narcissistic self-sorting in metal coordination.[42-45] However, most of these studies considering the narcissistic self-sorting of the structure as a whole, while the report focusing on narcissistic self-sorting used as self-recognition sites remains limited.[45-50] Furthermore, the homogeneous interactions in biological systems also prompted scientists to urgently develop ligand motifs for self-recognition.[51-52]

In this paper, to achieve coordination with high selectivity and specificity, we design two novel ortho-modified terpyridine ligands, i.e., **MA** and **MB** as model systems to form head-to-tail coordination complexes $\mathbf{Zn_2(MA)_2}$ and $\mathbf{Zn_3(MB)_2}$, respectively (Scheme 1b). The single-crystal structures of $\mathbf{Zn_2(MA)_2}$ and $\mathbf{Zn_3(MB)_2}$ show the non-coaxial feature of ortho-modified tpy after coordination, which is apparently different from the rotation of conventional tpy around its axis.[19, 53] Remarkably, **MA**, **MB**, and tpy mixture with Zn(II) could assemble into three distinct complexes $\mathbf{Zn_2(MA)_2}$, $\mathbf{Zn_3(MB)_2}$, and $\mathbf{Zn(tpy)_2}$, suggesting the narcissistic self-sorting behaviors. We then combined these moieties with tpy to form sterically congested multitopic ligands (**LA** and **LB**) for precise self-assembly of hexagonal macrocycles $\mathbf{Zn_9(LA)_6}$ and $\mathbf{Zn_{12}(LB)_6}$ (Scheme 1c). It's a common stragety to promote hierarchical assembly of metallacycles by introducing orthogonal interactions.[54-56] The tpy-based metallacycles could hierarchically self-assembly into hollow tubular or berry-type nanostructure through the face-to-face stacking according to the previous reports.[21, 57-59] Interestingly, it is found that the significantly steric

congestion and non-coaxial structure of **$Zn_9(LA)_6$** caused the restriction in the edging rotation of the hexagons, which further causes the hexagons to hierarchically assemble into giant cyclic nanostructures and metallogels via edge-to-edge stacking rather than face-to-face stacking.

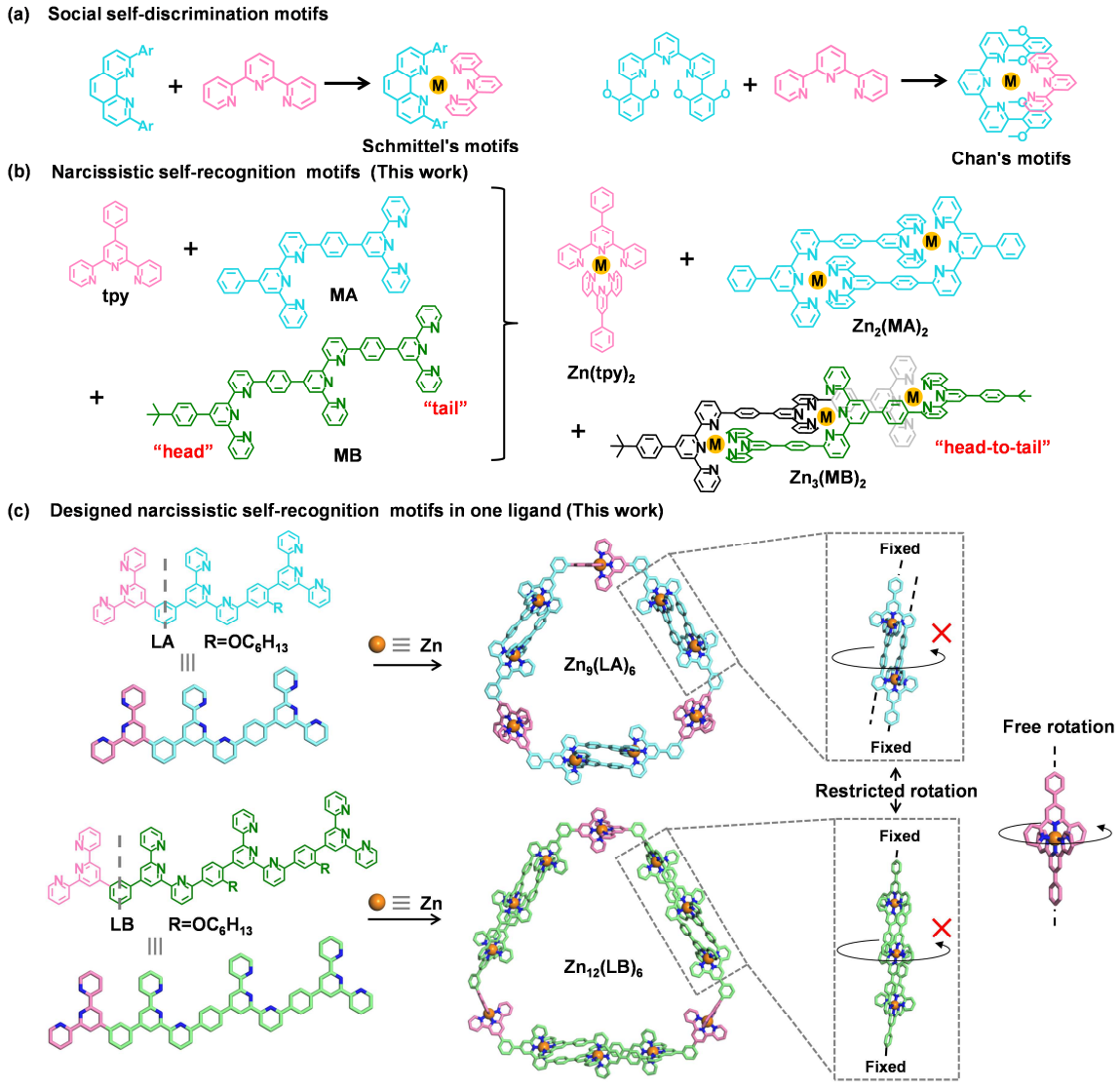

Scheme 1. (a) Social self-discrimination motifs in literatures. (b) Narcissistic self-recognition motifs in the current work. (c) Schematics for the self-assembly of complexes **$Zn_9(LA)_6$** and **$Zn_{12}(LB)_6$**.

Results and Discussion

Synthesis and characterization of model system MA and complex $Zn_2(MA)_2$. In our design, the modification at terpyridyl 6-position played a central role in the self-soring assembly. The simple and efficient synthesis process of **MA** only included a three-step reaction of the starting material, followed by the one-step purification of the product using column chromatography. Especially, the key compound 1 was synthesized by a typical Kröhnke reaction with pyridinium salt 5 (Scheme S1 in Supporting Information).[60] The final motif **MA** was obtained via Suzuki coupling reaction in a good yield (77%) and characterized by NMR and mass spectrometry (Figures S20 and S21). After that, **MA** and $Zn(NO_3)_2•6H_2O$ (with a precise stoichiometric ratio of 1:1, Figure 1a) were mixed in $CHCl_3$ and MeOH (1:3, v/v) at 50 °C for 12 h, followed by the addition of excessive NH_4PF_6 (to exchange NO_3^- with PF_6^-) in methanol to give a white precipitate $\mathbf{Zn_2(MA)_2}$ in a yield of 91%.

^{1}H NMR spectra of **MA** and complex $\mathbf{Zn_2(MA)_2}$ were shown in Figure 1b. Given the dissymmetrical nature of **MA**, five kinds of expected pyridines signals attributed to the terpyridinyl moieties were confirmed by 2D-COSY results (Figure S24). In the spectrum of complex $\mathbf{Zn_2(MA)_2}$, the peaks were sharp and well-resolved. The 2D-COSY and NOESY for $\mathbf{Zn_2(MA)_2}$ (Figures S57-S59) also showed five sets of pyridines signals as **MA**, suggesting a highly symmetrical structure of complex $\mathbf{Zn_2(MA)_2}$. Compared with **MA**, 6-position (6 and a6) signals of tpy were shifted upfield due to the electron shielding effect.[61] At the same time, the proton signals of e-tpy, f-Ph, and g-Ph were also shifted to upfield, which should be attributed to the existence of π-π interaction between tpy moiety and phenyl in the other ligand. In ESI-MS (Figure S1A), one prominent set of peaks with charge states from 2+ to 4+ was observed (due to the loss of different numbers of PF_6^-). After deconvolution, the molecular weight of complex $\mathbf{Zn_2(MA)_2}$ was 1940 Da, matching well with its expected chemical composition of two **MA** moieties, two Zn(II) ions and four PF_6^-. All the experimental isotope patterns agree excellently with the corresponding simulated isotope patterns (Figure S7). In traveling wave ion mobility-mass spectrometry (TWIM-MS),[23]

complex **$Zn_2(MA)_2$** showed a series of charge states with narrow drift time distribution ranging from 2+ to 4+, indicating the formation of a discrete product but without any isomers and conformers (Figure S1B).

To further confirm the structure, the single crystal of **$Zn_2(MA)_2$** was obtained by slowly diffusing the vapor of ethyl acetate into **$Zn_2(MA)_2$** in acetonitrile for over two weeks. As expected, X-ray crystallographic analysis (Figures 1c, 1d, and Movie S1) showed that two Zn(II) are sandwiched between two **MA** to form a dimer with the "head-to-tail" structure. The phenyl groups in the middle are parallel to each other (yellow part), and the distance between the two interlayers is 3.57 Å, indicating the existence of π-π interactions.[41, 62]

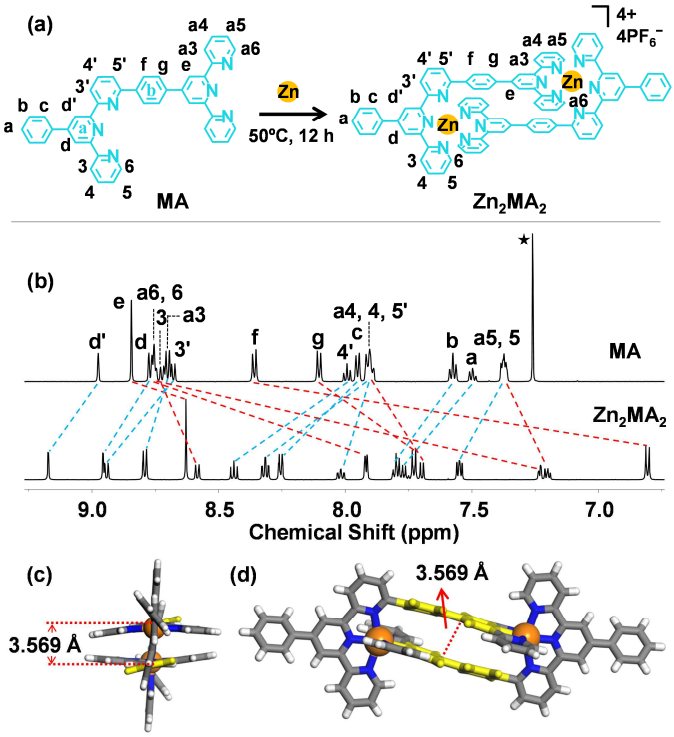

Figure 1. (a) The self-assembly of model system **MA** with Zn(II). (b) The ^{1}H NMR spectra (600 MHz, 300 K) of **MA** in $CDCl_3$ and complex **$Zn_2(MA)_2$** in CD_3CN. X-ray crystal structure in a (c) side view and (d) front view of complex **$Zn_2(MA)_2$**. Non-coordinated anions and solvent are omitted for clarity (C, gray or yellow; H, white; N, blue; Zn, orange).

Synthesis and characterization of model system MB and complex $Zn_3(MB)_2$. By referring to the synthetic and characterization procedures of **MA**, we further designed and obtain another model system **MB** (Figure 2a), which includes one additional tpy unit compared to **MA** and thereby exhibits an enhanced sterically congested effect. An extra *tert*-butyl was introduced to improve the solubility. tpy-based molecules have been extensively studied since the 1930s, however, it is worth noting that the unique structure of **MB**, has never been reported.[40, 63-64] The synthesis of **MB** (yield 75%) and self-assembly of complex $\mathbf{Zn_3(MB)_2}$ (yield 87%) (MB:Zn(II)=2:3) followed the same procedure as that of **MA** and $\mathbf{Zn_2(MA)_2}$.

The ^{1}H NMR data of **MB** and $\mathbf{Zn_3(MB)_2}$ were shown in Figure 2b. In the spectrum of **MB** with three tpy units, eight kinds of pyridines signals could be observed. Moreover, the complex $\mathbf{Zn_3(MB)_2}$ exhibited a more complicated structure and spectrum than $\mathbf{Zn_2(MA)_2}$, due to the enhanced steric hindrance effect caused by the introduction of the additional tpy unit. For each tpy, the differences in chemical shift ($\Delta\delta$) were 1.48 ppm and 0.8 ppm for 6 position proton and a6 proton, respectively, suggesting that the 6-position of a-tpy shows the strong shielding effect. The signals of tpy-3 and tpy-5 displayed upfield or downfield shifts after coordination, which were consistent with the previous studies.[65] In addition, the restrictive structure induced the split of NMR signals. Both the signals of the middle phenyls and tpy-b6 split into two sets of peaks, which indicate their rotation restriction caused by the altered chemical environment. ESI-MS (Figure S2A) and TWIM-MS (Figure S2B) spectra of $\mathbf{Zn_3(MB)_2}$ also exhibited a similar prominent set of peaks with different charge states and narrow drift time distribution ranging from 2+ to 4+, suggesting the formation of a single product without any overlapping isomers or conformers. The molecular weight of complex $\mathbf{Zn_3(MB)_2}$ (3020 Da) agrees well with its expected chemical composition of two **MB** ligands, three Zn(II) ions and six PF_6^-.

The single-crystal data of $\mathbf{Zn_3(MB)_2}$ was obtained by slowly diffusing the vapor of carbon tetrachloride into acetonitrile solution for over three weeks. Complex $\mathbf{Zn_3(MB)_2}$ also showed a sandwich-

like structure with a certain degree of distortion (Movie S2), suggesting higher steric congestion caused the helical shape (Figure 2c). The different distances between the two middle phenyls (yellow part) were 3.6 Å and 3.7 Å, respectively, which confirmed the helical structure. More importantly, under the sterically congested environment, the different tpy units coordinated with the same Zn(II) cannot maintain the vertical alignments and are forced to exhibit twisted structures. Furthermore, **$Zn_3(MB)_2$** has two chiral conformation due to the unique head-to-tail coordination mode, and both of the conformation could be found in single crystal (Figure S90).

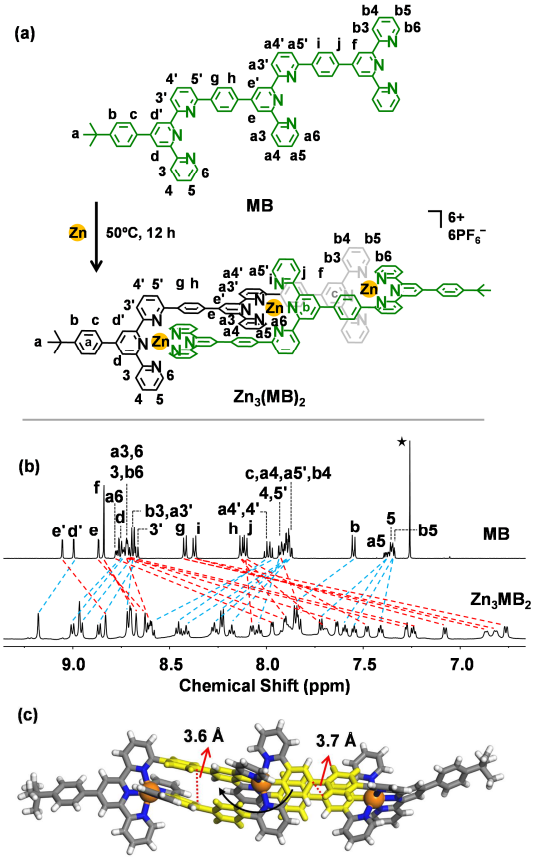

Figure 2. (a) The self-assembly of model system **MB** with Zn(II). (b) The ^{1}H NMR spectra (600 MHz, 300 K) of **MB** in $CDCl_3$ and **$Zn_3(MB)_2$** in CD_3CN. (c) X-ray crystal structure in a front view of

$Zn_3(MB)_2$. Non-coordinated anions and solvent are omitted for clarity (C, gray or yellow; H, white; N, blue; Zn, orange).

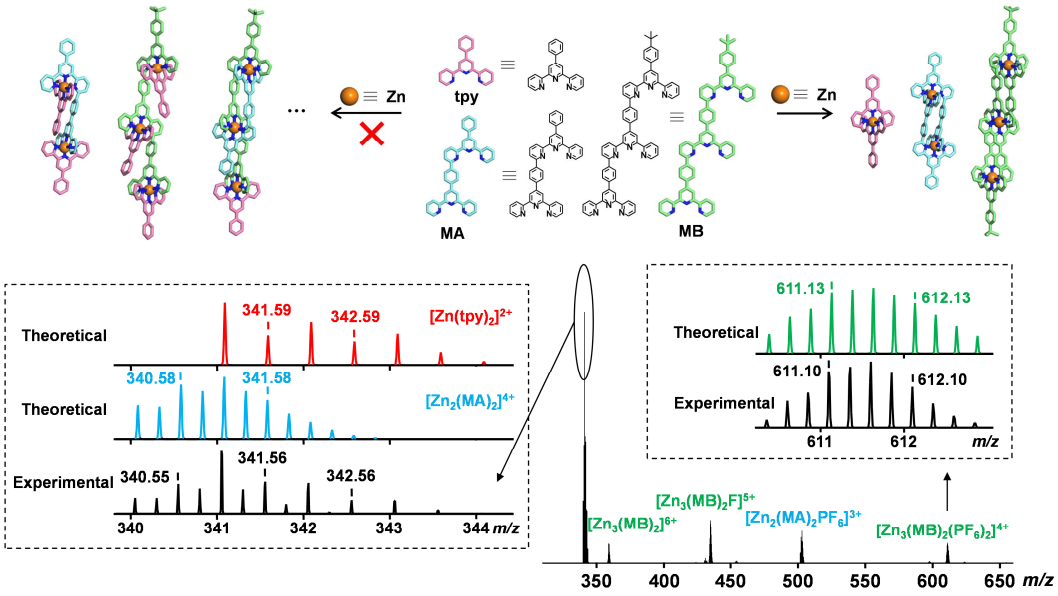

Figure 3. ESI-MS of the assembly of mixed **MA**, **MB**, and tpy with narcissistic self-sorting behavior.

Self-sorting behavior of MA, MB, and tpy. To evaluate the selectivity of these model systems, we investigated the self-sorting behavior of **MA**, **MB**, and conventional tpy.[66] In the self-sorting study, **MA**, **MB**, and conventional tpy were mixed together in an equimolar ratio with the corresponding amount of Zn(II) for the overnight self-assembly at 50 °C. ESI-MS clearly illustrated three sets of signals for the corresponding complexes but without statistical complexes (Figure 3), indicating that these model complexes exhibit ideal self-sorting properties in a pluralistic system. Both ESI-MS and NMR of any binary mixture (Figures S16-S18) showed independent signals for three complexes **$Zn_2(MA)_2$**, **$Zn_3(MB)_2$**, and **$Zn(tpy)_2$**, suggesting a characteristic narcissistic self-sorting.[29, 67-68] Moreover, we also monitored the kinetic process of narcissistic self-sorting, and the system basically reached equilibrium after 24 h (Figure S19). As expectation, in accord to the maximum occupancy of coordination sites proposed by Lehn,[69]

MA, **MB**, and tpy tend to narcissistically coordinate to form the most energy favorable structure. In this context, we are inspired to use **MA** and **MB** as self-recognition sites to further construct complex supramolecular structures.

Synthesis and self-assembly of ligands LA and LB with multiple tpy moieties. It is reported that the ditopic tpy ligands with 120° angle tend to self-assemble into a mixture of macrocycles with uncontrollable size and structure.[20] However, we expect that the dissymmetrical tritopic (**LA**) and tetratopic (**LB**) (Scheme 1c) ligands with 120° angle that contain narcissistic self-sorting moieties could be used to precisely construct complex supramolecular macrocycles $\mathbf{Zn_9(LA)_6}$ and $\mathbf{Zn_{12}(LB)_6}$. In order to improve the solubility of ligands, alkoxy chains (R=-OC_6H_{13}) were introduced. Compared with **LA** (yield, 76%), the synthesis of **LB** with one more tpy units turns to be significantly challenging. Fortunately, we successfully obtained **LB** (yield, 37%) by adding CH_3COOH/DMF as an auxiliary agent. The obtained ligands **LA** and **LB** were assembled into complexes $\mathbf{Zn_9(LA)_6}$ (yield, 86%) and $\mathbf{Zn_{12}(LB)_6}$ (yield, 84%) and were characterized by NMR, MALDI-TOF, ESI-MS, and TWIM-MS (Figures 4, S34-40, and S48-54).

Compared with **LA** and **LB**, ^{1}H NMR spectra of the complexes $\mathbf{Zn_9(LA)_6}$ (Movie S3) and $\mathbf{Zn_{12}(LB)_6}$ (Movie S4) were significantly broadened (Figure 4a), suggesting the assembly of large complexes with a slower tumbling on the NMR time scale.[24] Importantly, the peaks of pyridines on the b-tpy and c-tpy turn broader, due to the sterical congestion of the coordination units and the restriction in free rotation of the phenyl caused by the high steric congestion of alkoxy chains. In the spectrum of **LA**, seven kinds of expected pyridines signals were observed with respect to the tpy moieties. Owing to the continuous dissymmetrical modification of a- and b-tpy, **LB** displayed more complicated proton signals (i.e., ten distinguished kinds of pyridine peaks) than that of **LA** (Figure 4d). All 6 positions of pyridines were shifted towards upfield, because of the electron shielding effects after complexation. However, the chemical shifts of different protons differ significantly owing to the variable shielding strength. For

instance, the proton at a6 position showed a maximum chemical shift of Δδ= 1.41 ppm; while a slightly upfield-shift Δδ= 0.55 ppm was observed for b6 position. 2D-COSY and NOESY for two complexes **$Zn_9(LA)_6$** and **$Zn_{12}(LB)_6$** (Figures S70, S72 and S82, S84) also showed the same sets of tpy signals as ligands, suggesting the symmetrical structures of these two complexes. The diffusion-ordered NMR spectroscopy (DOSY) provided dimensional information for **$Zn_9(LA)_6$** and **$Zn_{12}(LB)_6$**. As shown in Figure S85, all proton signals appeared at the same band, indicating the formation of discrete assemblies. The diffusion coefficients in CD_3CN were log D= -9.61 for **$Zn_9(LA)_6$** and log D= -9.64 for **$Zn_{12}(LB)_6$**, respectively. The experimental hydrodynamic radii (rH) for **$Zn_9(LA)_6$** (2.4 nm) and **$Zn_{12}(LB)_6$** (2.6 nm) agreed well with the modeling structures.

In ESI-MS (Figure 4b and 4e), one prominent set of peaks with charge states (from 7+ to 14+ for **$Zn_9(LA)_6$** and from 8+ to 14+ for **$Zn_{12}(LB)_6$**) was observed on account of the loss of different numbers of PF_6^-. After deconvolution, the molecular weights of these two complexes were 8869 Da and 12974 Da, respectively, matching well with the expected chemical composition of **$Zn_9(LA)_6$** (6 **LA** ligands, 9 Zn(II) ions and 18 PF_6^-) and **$Zn_{12}(LB)_6$** (6 **LB** ligands, 12 Zn(II) ions and 24 PF_6^-). All the experimental isotope patterns agreed excellently with the corresponding simulated isotope patterns (Figures S9 and S10). Moreover, the TWIM-MS spectra of complexes **$Zn_9(LA)_6$** and **$Zn_{12}(LB)_6$** also showed narrow drift time distribution, supporting the formation of single species with rigid structures (Figures 4c, 4f). The full characterization of NMR, ESI-MS, and TWIM-MS confirmed that the two types of tpy moieties in ligands **LA** and **LB** could precisely self-assemble into hexagonal macrocycles through the narcissistic self-recognition mechanism. Such moieties with high coordination selectivity and specificity may find their potential in the constructions of more complex metallo-supramolecules with precisely controlled shapes and sizes.

Interestingly, when complexes **$Zn_9(LA)_6$** and **$Zn_{12}(LB)_6$** were mixed in an equimolar ratio at 50 °C for overnight, ESI-MS and TWIM-MS clearly illustrated two additional sets of signals besides **$Zn_9(LA)_6$**

and **$Zn_{12}(LB)_6$** (Figure S6). The compositions of **$Zn_{10}(LA)_4(LB)_2$** and **$Zn_{11}(LA)_2(LB)_4$** (Figures S14 and S15) were confirmed by analyzing the ESI-MS and TWIM-MS data. No exchange for odd number ligands was observed in this mixture, suggesting that it could be a sub-component exchange based on the dominant coordination dimer rather than the usual ligand exchange.[70-71] It indicated that the dimer structures based on ditopic and tritopic tpy moieties not only exhibit higher selectivity but also show higher stability than single-tpy unit.

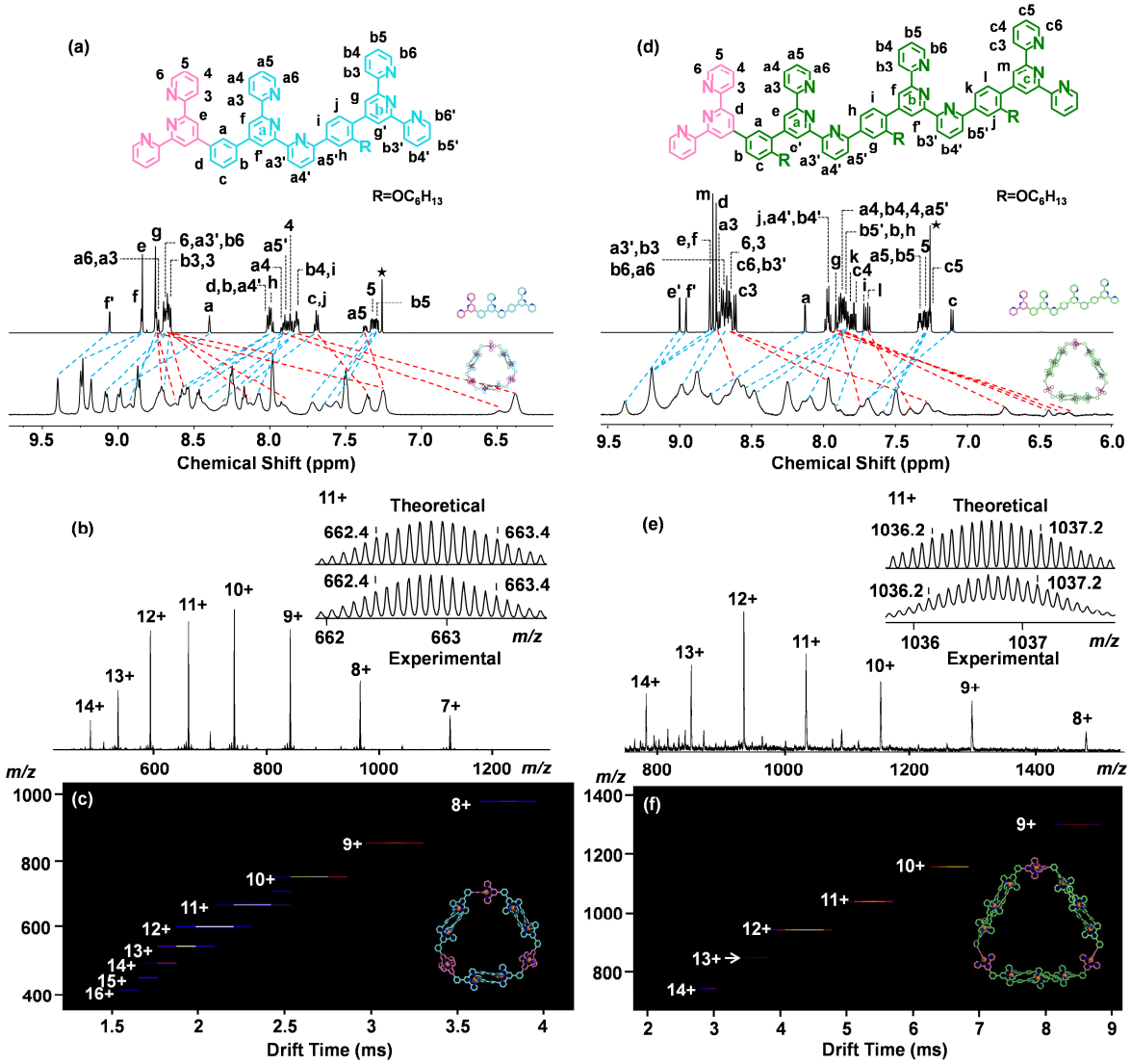

Figure 4. (a) ^{1}H NMR spectra (600 MHz, 300 K) of ligand **LA** in $CDCl_3$ (top) and hexagon $\mathbf{Zn_9(LA)_6}$ in CD_3CN (bottom). (b) ESI-MS and (c) TWIM-MS plots (*m/z* vs drift time) of $\mathbf{Zn_9(LA)_6}$. (d) ^{1}H NMR spectra (600 MHz, 300 K) of ligand **LB** in $CDCl_3$ (top) and hexagon $\mathbf{Zn_{12}(LB)_6}$ in CD_3CN (bottom). (e) ESI-MS and (f) TWIM-MS plots (*m/z* vs drift time) of $\mathbf{Zn_{12}(LB)_6}$.

Hierarchical self-assembly. Our study shows that, with increasing the concentration of $\mathbf{Zn_9(LA)_6}$ and $\mathbf{Zn_{12}(LB)_6}$ in acetonitrile at room temperature, both of the solutions could form metallogels at a concentration of 45 mg/mL for $\mathbf{Zn_9(LA)_6}$ and 25 mg/mL for $\mathbf{Zn_{12}(LB)_6}$ (Figure 6d). The gels were also temperature-responsive, and could be converted into solutions after heating at 50 ^{o}C for 1 h. To explore the mechanism of gelation, we then used TEM to investigate the morphology of $\mathbf{Zn_9(LA)_6}$ and $\mathbf{Zn_{12}(LB)_6}$ at different concentrations. At low concentrations (10^{-6} M), the assemblies were almost distributed in a monodispersed manner. Both complexes exhibited unique hollow structures, suggesting high rigidity, stability and large inner space. The measured sizes of the two complexes were 5.5 nm for $\mathbf{Zn_9(LA)_6}$ and 6.5 nm for $\mathbf{Zn_{12}(LB)_6}$, respectively (Figures 5b and 6a). However, at a high concentration (10^{-5} M), some giant cyclic nanostructures in larger size were observed (Figure 5c). The diameters of these structures were much larger than that of individual $\mathbf{Zn_9(LA)_6}$, implying the clustering of $\mathbf{Zn_9(LA)_6}$. The height of the hierarchically assembled nanostructures measured by the AFM image (Figures 5e and 5f) was about 1.5 nm, which was very close to the height of the monolayer. When the concentration further increased, these giant macrocycles formed a three-dimensional cross-linked network via intermolecular interaction (Figure 5d). For $\mathbf{Zn_{12}(LB)_6}$ with a larger size, although the similar monolayer nanostructures were observed (Figure 6b), the degree of aggregation was significantly increased. Further, at a much higher concentration of 10^{-4} M, the formed giant macrocycles showed obvious vertical stacking in space (Figure 6c).

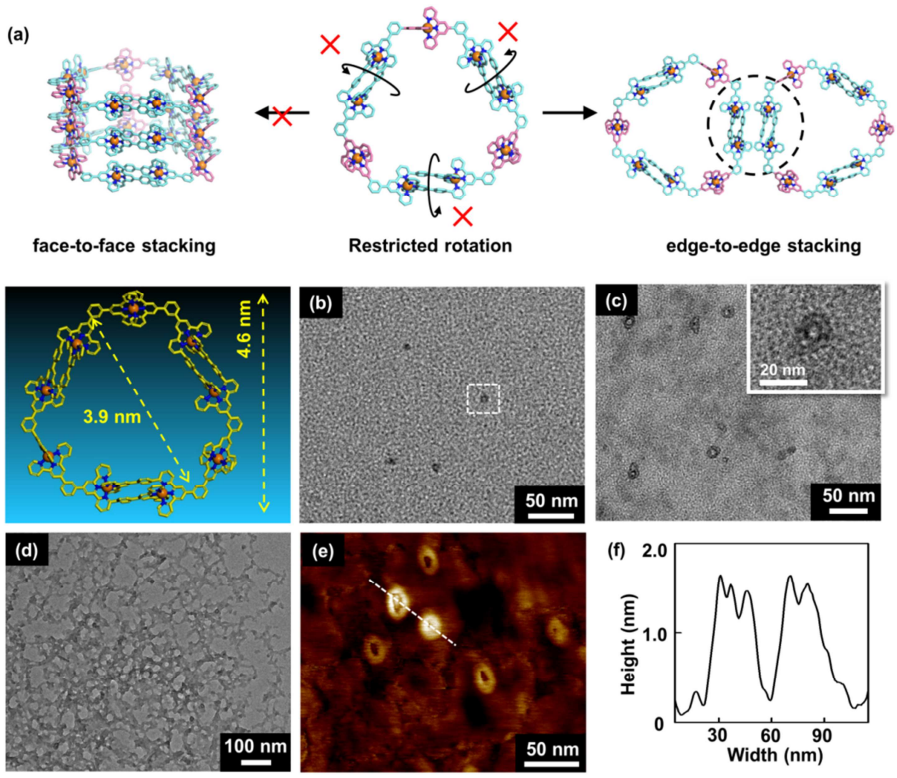

Figure 5. (a) Schematic diagram of edge-to-edge stacking by $\mathbf{Zn_9(LA)_6}$. TEM images of (b) individual $\mathbf{Zn_9(LA)_6}$ (the energy-minimized structure from molecular modeling at left), (c) assembled cyclic nanostructures of $\mathbf{Zn_9(LA)_6}$ (zoomed-in image in inset, scale bar was 20 nm), (d) 3D network structure formed by assembled cyclic nanostructures of $\mathbf{Zn_9(LA)_6}$, (e) AFM images of hierarchically assembled cyclic nanostructures by $\mathbf{Zn_9(LA)_6}$, (f) cross-section of the cyclic nanostructure shown in image e.

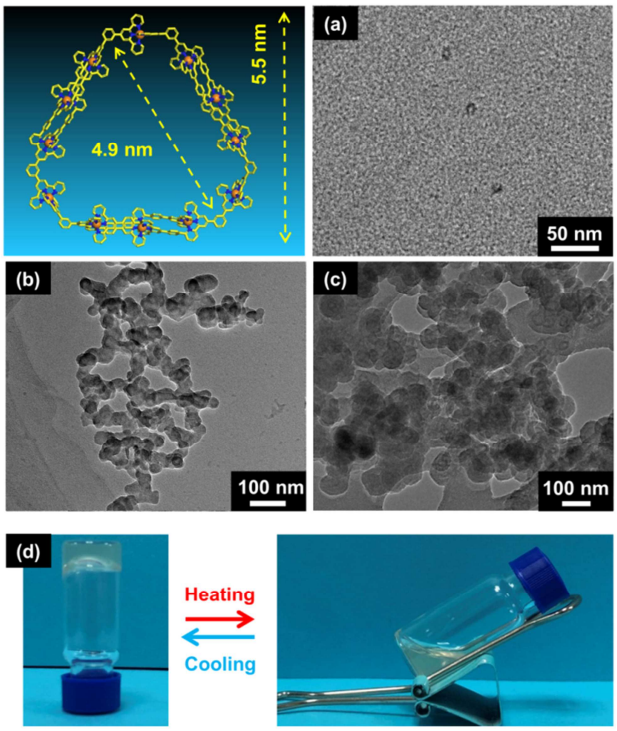

Figure 6. TEM images of (a) individual $\mathbf{Zn_{12}(LB)_6}$ (the energy-minimized structure from molecular modeling at left), (b) assembled cyclic nanostructures of $\mathbf{Zn_{12}(LB)_6}$, (c) 3D network structure formed by assembled cyclic nanostructures of $\mathbf{Zn_{12}(LB)_6}$ and (d) photograph of $\mathbf{Zn_{12}(LB)_6}$ gel formation in CH_3CN.

As well-known, the <tpy-M(II)-tpy> unit could rotate freely around the axis without space obstruction. However, due to the special spatially complementary coordination of **LA** and **LB**, these two axial dissymmetrical ligands exhibited entirely steric congestions. Therefore, it can be inferred that the hexagons are basically composed of vertical edges, since the rotation of the dimer can result in the disassembly (Figure 5a). In order to study the edge-to-edge stacking of $\mathbf{Zn_9(LA)_6}$, we tried to grow single crystal of $\mathbf{Zn_9(LA)_6}$. However, all efforts to grow single crystal of $\mathbf{Zn_9(LA)_6}$ has proven to be unsuccessful. Instead, we synthesised a model ligand $\mathbf{MA\text{-}OC_6H_{13}}$ (Scheme S2 in Supporting Information) and further got the complex $\mathbf{Zn_2(MA\text{-}OC_6H_{13})_2}$ which has exactly the same structure as the ditopic part of $\mathbf{Zn_9(LA)_6}$. The single-crystal packing of $\mathbf{Zn_2(MA\text{-}OC_6H_{13})_2}$ provided the strong evidence

for the edge-to-edge stacking of **$Zn_9(LA)_6$**. As shown in Figure 7, the intermolecular packing of **$Zn_2(MA\text{-}OC_6H_{13})_2$** is more compact than that of **$Zn_2(MA)_2$** (Figure S91), which indicated that the introduction of alkyl chains can enhance the intermolecular interactions. The distance between pyridine and central phenyl of another molecular is 3.8 Å, which indicated the existence of π-π interaction. The distance between the alkyl chain and central phenyl of another molecular is 2.6 Å, which indicated the existence of CH-π interactions. Since **$Zn_{12}(LB)_6$** could provide additional sites in the vertical direction than complex **$Zn_9(LA)_6$**, **$Zn_{12}(LB)_6$** is hard to find the discrete cyclic nanostructures as that of **$Zn_9(LA)_6$**.

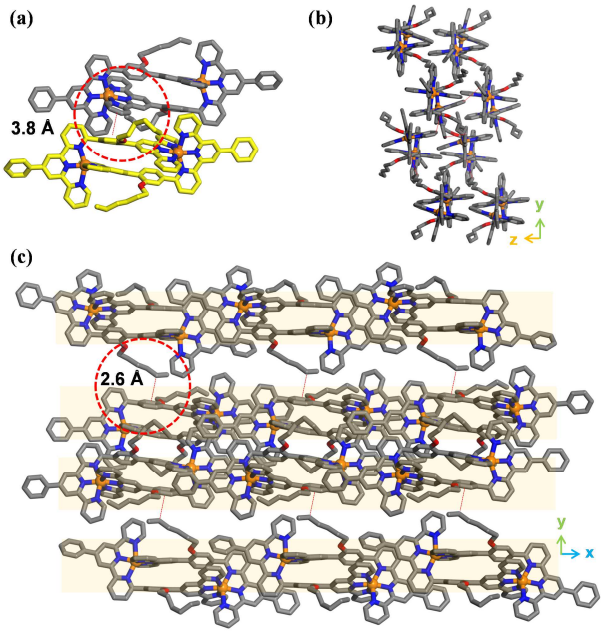

Figure 7. (a) Crystal packing of complex **$Zn_2(MA\text{-}OC_6H_{13})_2$** and (b), (c) 2D stacking diagram of **$Zn_2(MA\text{-}OC_6H_{13})_2$**. H atoms, non-coordinated anions and solvent are omitted for clarity (C, gray or yellow; N, blue; Zn, orange).

Photophysical Properties. Considering the enhanced conjugation and restricted rotation of the structures, we further investigated UV/Vis absorption and photoluminescence of all ligands and complexes in solution state (10^{-6} M). As shown in Figure 8a, compared with the absorption spectra of ligands (Figure S88), all complexes displayed a significant redshift which originating from intra-ligand charge transfer (ILCT).[72] In sharp contrast with **$Zn(tpy)_2$**, the maximum emission wavelength of

$Zn_2(MA)_2$ displayed a ca. 75 nm redshift, ascribed to the enhanced conjugation (Figure 8b). However, complex **$Zn_3(MB)_2$** with more complicated structure also showed similar maximum emission wavelength to **$Zn_2(MA)_2$**, the reason should be the twisted structures induced the conjugation. For hexagonal macrocycles **$Zn_9(LA)_6$** and **$Zn_{12}(LB)_6$**, the restrictive intramolecular rotation in the congested and non-coaxial structures caused further enhance of their fluorescence intensity. Moreover, due to the introduction of alkoxy chains as electron donor, the maximum emission peaks of **$Zn_9(LA)_6$** and **$Zn_{12}(LB)_6$** exhibited 20 nm red shifted than that of **$Zn_2(MA)_2$** and **$Zn_3(MB)_2$**.

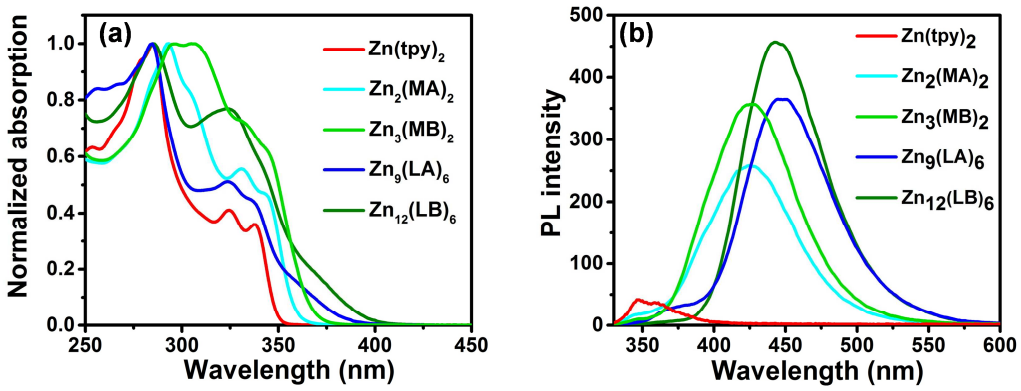

Figure 8. (a) UV/Vis absorption and (b) PL spectra of all complexes (10^{-6} M in CH_3CN, λ_e = 325 nm).

Conclusion

In summary, we have designed and synthesized a series of multitopic tpy ligands with designed coordination selectivity by ortho-modification. As shown by the single-crystal detections, the model systems **MA** and **MB** can assemble into head-to-tail coordination complexes **$Zn_2(MA)_2$** and **$Zn_3(MB)_2$**, respectively. Moreover, the assembly of mixtures of **MA**, **MB**, and **tpy** exhibit excellent selectivity due to the narcissistic self-sorting mechanism. Further, we introduced these moieties with high selectivity into multitopic ligands **LA** and **LB,** which were used to further precisely construct the hexagonal metallo-supramolecules. Such a design caused the restriction in rotations of the hexagons, which further leads to their hierarchical assembly into giant cyclic nanostructures and metallogels. Moreover, these complexes

showed significantly enhanced fluorescence intensity in solution state than the complexes based on conventional tpy. Our design and fabrication of dissymmetrical coordination moieties could pave a new avenue for the development of a set of congested coordination pairs with high selectivity and specificity for the assembly of sequence-specific metallo-supramolecular architectures.

Acknowledgements

We gratefully acknowledge the support from the National Natural Science Foundation of China (22071079 for M.W), the Natural Science Foundation of Jilin Province (20180101297JC for M. W.) and the staffs from BL17B beamline of National Facility for Protein Science in Shanghai (NFPS) at Shanghai Synchrotron Radiation Facility for assistance during data collection.

Author contributions

M.W. conceived and designed the experiments. J.M and K.L completed the synthesis. J.M, T.L., Y.X, Z.L., J.S, Q.B., Z.Z., X.-Q.H, Z.C. and P.W conducted the characterization. J.M, T.L. X.D., and M.W. analysed the data and wrote the manuscript. All the authors discussed the results and commented on and proofread the manuscript.

Additional information

Supplementary Information: Synthetic details; characterizations of ligands and complexes including NMR, ESI-MS, TWIM-MS and single crystals.

Competing interests: The authors declare no competing financial interests.

References

1. Lehn J-M. From supramolecular chemistry towards constitutional dynamic chemistry and adaptive chemistry. *Chem. Soc. Rev.,* **36**, 151-160 (2007).

2. Chakrabarty R, Mukherjee PS, Stang PJ. Supramolecular coordination: self-assembly of finite two- and three-dimensional ensembles. *Chem. Rev.,* **111**, 6810-6918 (2011).

3. Cook TR, Stang PJ. Recent Developments in the Preparation and Chemistry of Metallacycles and Metallacages via Coordination. *Chem. Rev.,* **115**, 7001-7045 (2015).

4. Chakraborty S, Newkome GR. Terpyridine-based metallosupramolecular constructs: tailored monomers to precise 2D-motifs and 3D-metallocages. *Chem. Soc. Rev.,* **47**, 3991-4016 (2018).

5. Olenyuk B, Whiteford JA, Fechtenkötter A, Stang PJ. Self-assembly of nanoscale cuboctahedra by coordination chemistry. *Nature* **398**, 796-799 (1999).

6. Fujita D, Ueda Y, Sato S, Mizuno N, Kumasaka T, Fujita M. Self-assembly of tetravalent Goldberg polyhedra from 144 small components. *Nature* **540**, 563-566 (2016).

7. Sun QF*, et al.* Self-assembled M24L48 polyhedra and their sharp structural switch upon subtle ligand variation. *Science* **328**, 1144-1147 (2010).

8. Danon JJ*, et al.* Braiding a molecular knot with eight crossings. *Science* **355**, 159 (2017).

9. Newkome GR*, et al.* Nanoassembly of a fractal polymer: a molecular "Sierpinski hexagonal gasket". *Science* **312**, 1782-1785 (2006).

10. Zhang Y-Y, Gao W-X, Lin L, Jin G-X. Recent advances in the construction and applications of heterometallic macrocycles and cages. *Coord. Chem. Rev.,* **344**, 323-344 (2017).

11. Goswami A, Schmittel M. Heteroleptic copper phenanthroline complexes in motion: From stand-alone devices to multi-component machinery. *Coord. Chem. Rev.,* **376**, 478-505 (2018).

12. Tai C-Y, Fu J-H, Lee Y-H, He Y-J, Wang S-C, Chan Y-T. Facile synthesis of multicomponent heterobimetallic metallomacrocycles through selective metal–ligand coordination. *Chem. Commun.,* **55**, 6289-6292 (2019).

13. Hiraoka S, Kubota Y, Fujita M. Self- and hetero-recognition in the guest-controlled assembly of Pd(ii)-linked cages from two different ligands. *Chem. Commun.*, 1509-1510 (2000).

14. Zhao L*, et al.* Self-Selection in the Self-Assembly of Isomeric Supramolecular Squares from Unsymmetrical Bis(4-pyridyl)acetylene Ligands. *J. Org. Chem.,* **73**, 6580-6586 (2008).

15. Yin GQ*, et al.* Self-assembly of emissive supramolecular rosettes with increasing complexity using multitopic terpyridine ligands. *Nat. Commun.,* **9**, 567 (2018).

16. Wei C, He Y, Shi X, Song Z. Terpyridine-metal complexes: Applications in catalysis and supramolecular chemistry. *Coord. Chem. Rev.,* **385**, 1-19 (2019).

17. Bode S*, et al.* Self-healing polymer coatings based on crosslinked metallosupramolecular copolymers. *Adv. Mater.,* **25**, 1634-1638 (2013).

18. Eryazici I, Moorefield CN, Newkome GR. Square-Planar Pd(II), Pt(II), and Au(III) Terpyridine Complexes: Their Syntheses, Physical Properties, Supramolecular Constructs, and Biomedical Activities. *Chem. Rev.,* **108**, 1834-1895 (2008).

19. Newkome GR, Moorefield CN. From 1 --> 3 dendritic designs to fractal supramacromolecular constructs:

understanding the pathway to the Sierpinski gasket. *Chem. Soc. Rev.,* **44**, 3954-3967 (2015).

20. Li X*, et al.* Separation and characterization of metallosupramolecular libraries by ion mobility mass spectrometry. *Anal. Chem.,* **83**, 6667-6674 (2011).

21. Shi J*, et al*. Self-Assembly of Metallo-Supramolecules with Dissymmetrical Ligands and Characterization by Scanning Tunneling Microscopy. *J. Am. Chem. Soc.,* **143**, 1224-1234 (2021).

22. Chan Y-T, Li X, Moorefield CN, Wesdemiotis C, Newkome GR. Towards larger polygonal architectures: synthesis and characterization of iron(II)- and ruthenium(II)-bis(terpyridine) metallomacrocycles. *Chemistry* **17**, 7750-7754 (2011).

23. Chan Y-T*, et al.* Design, synthesis, and traveling wave ion mobility mass spectrometry characterization of iron(II)- and ruthenium(II)-terpyridine metallomacrocycles. *J. Am. Chem. Soc.,* **133**, 11967-11976 (2011).

24. Zhang Z*, et al.* Intra- and intermolecular self-assembly of a 20-nm-wide supramolecular hexagonal grid. *Nat. Chem.,* **12**, 468-474 (2020).

25. Jiang Z*, et al.* Self-assembly of a supramolecular hexagram and a supramolecular pentagram. *Nat. Commun.,* **8**, 15476 (2017).

26. Fu J-H, Wang S-Y, Chen Y-S, Prusty S, Chan Y-T. One-Pot Self-Assembly of Stellated Metallosupramolecules from Multivalent and Complementary Terpyridine-Based Ligands. *J. Am. Chem. Soc.,* **141**, 16217-16221 (2019).

27. Jiang Z*, et al.* Precise Self-Assembly of Molecular Four- and Six-Pointed Stars. *Inorg. Chem.,* **59**, 875-879 (2020).

28. Andersen ES*, et al.* Self-assembly of a nanoscale DNA box with a controllable lid. *Nature* **459**, 73-76 (2009).

29. Wu A, Isaacs L. Self-Sorting: The Exception or the Rule? *J. Am. Chem. Soc.,* **125**, 4831-4835 (2003).

30. Acharyya K, Mukherjee S, Mukherjee PS. Molecular Marriage through Partner Preferences in Covalent Cage Formation and Cage-to-Cage Transformation. *J. Am. Chem. Soc.,* **135**, 554-557 (2013).

31. Jiménez A, Bilbeisi RA, Ronson TK, Zarra S, Woodhead C, Nitschke JR. Selective Encapsulation and Sequential Release of Guests Within a Self-Sorting Mixture of Three Tetrahedral Cages. *Angew. Chem. Int. Ed.,* **53**, 4556-4560 (2014).

32. Yamanaka M, Yamada Y, Sei Y, Yamaguchi K, Kobayashi K. Selective Formation of a Self-Assembling Homo or Hetero Cavitand Cage via Metal Coordination Based on Thermodynamic or Kinetic Control. *J. Am. Chem. Soc.,* **128**, 1531-1539 (2006).

33. Sun QF, Sato S, Fujita M. An $M_{12}(L(1))_{12}(L(2))_{12}$ cantellated tetrahedron: a case study on mixed-ligand self-assembly. *Angew. Chem. Int. Ed. Engl.,* **53**, 13510-13513 (2014).

34. Mahata K, Saha ML, Schmittel M. From an Eight-Component Self-Sorting Algorithm to a Trisheterometallic Scalene Triangle. *J. Am. Chem. Soc.,* **132**, 15933-15935 (2010).

35. Wang S-C, Cheng K-Y, Fu J-H, Cheng Y-C, Chan Y-T. Conformational Regulation of Multivalent Terpyridine

Ligands for Self-Assembly of Heteroleptic Metallo-Supramolecules. *J. Am. Chem. Soc.,* **142**, 16661-16667 (2020).

36. De S, Mahata K, Schmittel M. Metal-coordination-driven dynamic heteroleptic architectures. *Chem. Soc. Rev.,* **39**, 1555-1575 (2010).

37. Wang S-Y, Fu J-H, Liang Y-P, He Y-J, Chen Y-S, Chan Y-T. Metallo-Supramolecular Self-Assembly of a Multicomponent Ditrigon Based on Complementary Terpyridine Ligand Pairing. *J. Am. Chem. Soc.,* **138**, 3651-3654 (2016).

38. Goswami A, Saha S, Biswas PK, Schmittel M. (Nano)mechanical Motion Triggered by Metal Coordination: from Functional Devices to Networked Multicomponent Catalytic Machinery. *Chem. Rev.,* **120**, 125-199 (2020).

39. Swiegers GF, Malefetse TJ. New Self-Assembled Structural Motifs in Coordination Chemistry. *Chem. Rev.,* **100**, 3483-3538 (2000).

40. Hofmeier H, Schubert US. Recent developments in the supramolecular chemistry of terpyridine-metal complexes. *Chem. Soc. Rev.,* **33**, 373-399 (2004).

41. Constable EC. 2,2':6',2''-terpyridines: from chemical obscurity to common supramolecular motifs. *Chem. Soc. Rev.,* **36**, 246-253 (2007).

42. Pinalli R*, et al.* Cavitand-Based Nanoscale Coordination Cages. *J. Am. Chem. Soc.,* **126**, 6516-6517 (2004).

43. Caulder DL, Raymond KN. Superamolecular Self-Recognition and Self-Assembly in Gallium(III) Catecholamide Triple Helices. *Angew. Chem. Int. Ed. Engl.,* **36**, 1440-1442 (1997).

44. Taylor PN, Anderson HL. Cooperative Self-Assembly of Double-Strand Conjugated Porphyrin Ladders. *J. Am. Chem. Soc.,* **121**, 11538-11545 (1999).

45. Rizzuto FJ, Nitschke JR. Narcissistic, Integrative, and Kinetic Self-Sorting within a System of Coordination Cages. *J. Am. Chem. Soc.,* **142**, 7749-7753 (2020).

46. Safont-Sempere MM, Fernández G, Würthner F. Self-Sorting Phenomena in Complex Supramolecular Systems. *Chem. Rev.,* **111**, 5784-5814 (2011).

47. He Z, Jiang W, Schalley CA. Integrative self-sorting: a versatile strategy for the construction of complex supramolecular architecture. *Chem. Soc. Rev.,* **44**, 779-789 (2015).

48. Ghosh A, Schmittel M. Using multiple self-sorting for switching functions in discrete multicomponent systems. *Beilstein J. Org. Chem.,* **16**, 2831-2853 (2020).

49. Zheng Y-R, Yang H-B, Northrop BH, Ghosh K, Stang PJ. Size Selective Self-Sorting in Coordination-Driven Self-Assembly of Finite Ensembles. *Inorg. Chem.,* **47**, 4706-4711 (2008).

50. Johnson AM*, et al.* Narcissistic Self-Sorting in Self-Assembled Cages of Rare Earth Metals and Rigid Ligands. *Angew. Chem. Int. Ed.,* **54**, 5641-5645 (2015).

51. Rubinstein R*, et al.* Molecular Logic of Neuronal Self-Recognition through Protocadherin Domain

Interactions. *Cell* **163**, 629-642 (2015).

52. Goodman Kerry M*, et al.* Structural Basis of Diverse Homophilic Recognition by Clustered α- and β-Protocadherins. *Neuron* **90**, 709-723 (2016).

53. Wild A, Winter A, Schlutter F, Schubert US. Advances in the field of pi-conjugated 2,2':6',2''-terpyridines. *Chem. Soc. Rev.,* **40**, 1459-1511 (2011).

54. Datta S, Saha ML, Stang PJ. Hierarchical Assemblies of Supramolecular Coordination Complexes. *Acc. Chem. Res.,* **51**, 2047-2063 (2018).

55. Sun Y, Chen C, Stang PJ. Soft Materials with Diverse Suprastructures via the Self-Assembly of Metal-Organic Complexes. *Acc. Chem. Res.,* **52**, 802-817 (2019).

56. Sepehrpour H, Fu W, Sun Y, Stang PJ. Biomedically Relevant Self-Assembled Metallacycles and Metallacages. *J. Am. Chem. Soc.,* **141**, 14005-14020 (2019).

57. Song B*, et al.* Self-assembly of polycyclic supramolecules using linear metal-organic ligands. *Nat. Commun.,* **9**, 4575 (2018).

58. Yin G-Q*, et al.* Self-assembly of emissive supramolecular rosettes with increasing complexity using multitopic terpyridine ligands. *Nat. Commun.,* **9**, 567 (2018).

59. Chen M*, et al.* Highly Stable Spherical Metallo-Capsule from a Branched Hexapodal Terpyridine and Its Self-Assembled Berry-type Nanostructure. *J. Am. Chem. Soc.,* **140**, 2555-2561 (2018).

60. KrÖHnke F. The Specific Synthesis of Pyridines and Oligopyridines. *Synthesis* **1976**, 1-24 (1976).

61. Wang JL*, et al.* Stoichiometric self-assembly of shape-persistent 2D complexes: a facile route to a symmetric supramacromolecular spoked wheel. *J. Am. Chem. Soc.,* **133**, 11450-11453 (2011).

62. Grimme S. Do Special Noncovalent π–π Stacking Interactions Really Exist? *Angew. Chem. Int. Ed. Engl.,* **47**, 3430-3434 (2008).

63. Cargill Thompson AMW. The synthesis of 2,2':6',2''-terpyridine ligands — versatile building blocks for supramolecular chemistry. *Coord. Chem. Rev.,* **160**, 1-52 (1997).

64. Housecroft CE, Constable EC. The terpyridine isomer game: from chelate to coordination network building block. *Chem. Commun.,* **56**, 10786-10794 (2020).

65. Wang M*, et al.* Hexagon Wreaths: Self-Assembly of Discrete Supramolecular Fractal Architectures Using Multitopic Terpyridine Ligands. *J. Am. Chem. Soc.,* **136**, 6664-6671 (2014).

66. Heller M, Schubert US. Syntheses of Functionalized 2,2′:6′,2′′-Terpyridines. *ChemInform* **34**, (2003).

67. Lal Saha M, Schmittel M. Degree of molecular self-sorting in multicomponent systems. *Org. Biomol. Chem.,* **10**, 4651-4684 (2012).

68. Wang M*, et al.* From Trigonal Bipyramidal to Platonic Solids: Self-Assembly and Self-Sorting Study of Terpyridine-Based 3D Architectures. *J. Am. Chem. Soc.,* **136**, 10499-10507 (2014).

69. Kramer R, Lehn JM, Marquis-Rigault A. Self-recognition in helicate self-assembly: spontaneous formation of helical metal complexes from mixtures of ligands and metal ions. *Proc. Natl. Acad. Sci. U. S. A.* **90**, 5394 (1993).

70. Sato S, Ishido Y, Fujita M. Remarkable Stabilization of $M_{12}L_{24}$ Spherical Frameworks through the Cooperation of 48 Pd(II)−Pyridine Interactions. *J. Am. Chem. Soc.,* **131**, 6064-6065 (2009).

71. Wang L*, et al.* Introducing Seven Transition Metal Ions into Terpyridine-Based Supramolecules: Self-Assembly and Dynamic Ligand Exchange Study. *J. Am. Chem. Soc.,* **142**, 1811-1821 (2020).

72. Wang X-y, Del Guerzo A, Schmehl RH. Preferential solvation of an ILCT excited state in bis(terpyridine–phenylene–vinylene) Zn(ii) complexes. *Chem. Commun.*, 2344-2345 (2002).

Supplementary Files

This is a list of supplementary files associated with this preprint. Click to download.

- SupportingInformation.pdf
- MovieS1.mp4
- MovieS2.mp4
- MovieS3.mp4
- MovieS4.mp4
- Zn2MA2.cif
- Zn2MAOC6H132.cif
- Zn3MB2.cif